



Delft University of Technology

Analysis of Stochasticity and Heterogeneity of Car-Following Behavior Based on Data-Driven Modeling

Shiomi, Yasuhiro; Li, Guopeng; Knoop, Victor L.

DOI

[10.1177/03611981231169279](https://doi.org/10.1177/03611981231169279)

Publication date

2023

Document Version

Final published version

Published in

Transportation Research Record

Citation (APA)

Shiomi, Y., Li, G., & Knoop, V. L. (2023). Analysis of Stochasticity and Heterogeneity of Car-Following Behavior Based on Data-Driven Modeling. *Transportation Research Record*, 2677(12), 604-619. <https://doi.org/10.1177/03611981231169279>

Important note

To cite this publication, please use the final published version (if applicable). Please check the document version above.

Copyright

Other than for strictly personal use, it is not permitted to download, forward or distribute the text or part of it, without the consent of the author(s) and/or copyright holder(s), unless the work is under an open content license such as Creative Commons.

Takedown policy

Please contact us and provide details if you believe this document breaches copyrights. We will remove access to the work immediately and investigate your claim.

Green Open Access added to TU Delft Institutional Repository

'You share, we take care!' - Taverne project

<https://www.openaccess.nl/en/you-share-we-take-care>

Otherwise as indicated in the copyright section: the publisher is the copyright holder of this work and the author uses the Dutch legislation to make this work public.

Analysis of Stochasticity and Heterogeneity of Car-Following Behavior Based on Data-Driven Modeling

Transportation Research Record
2023, Vol. 2677(12) 604–619
© National Academy of Sciences:
Transportation Research Board 2023
Article reuse guidelines:
sagepub.com/journals-permissions
DOI: 10.1177/03611981231169279
journals.sagepub.com/home/trr
S Sage

Yasuhiro Shiomi¹ , Guopeng Li² , and Victor L. Knoop² 

Abstract

Traffic dynamics on freeways are stochastic in nature because of errors in perception and operation of drivers as well as the heterogeneity between and within drivers. This stochasticity is often represented in car-following models by a stochastic term, which is assumed to follow a normal distribution for the convenience of mathematical processing. However, the validity of this assumption has not been studied yet. In this study, we focused on the shape of the distribution of a stochastic term in the car-following model that predicts an acceleration after a time step. Based on vehicle trajectory data on a freeway in Japan, a car-following model is first developed by using data-driven methodology in which long short-term memory (LSTM) network is applied. In this LSTM network, the acceleration value is discretized and the model parameters are trained with the focal loss function. The relationship between the predicted distributions' modality, standard deviation (SD), and I_A with respect to traffic states is then examined. The findings demonstrate that: 1) the developed model can accurately predict the accelerations; 2) a probabilistic distribution tends to have a large SD and multimodality around a merging point and at the beginning of and along stop-and-go waves; and 3) driving behavior can be classed in one of four clusters based on the variation of the percentile value that a driver takes within the probability distribution. The proposed model and the insights are helpful for improving microscopic simulation models when considering new traffic management measures.

Keywords

operations, car-following, microscopic traffic models, models, simulation, traffic flow

To develop a workable traffic management and control strategy, it is imperative to comprehend the nature of traffic flow dynamics. Traffic dynamics are stochastic in nature. Since the beginning of traffic flow analysis, a great deal of research attention has been given to the stochasticity of traffic flow (e.g., Haight) (1). Initially, numerous studies were conducted to ascertain the shape of the distribution of indices representing the state of a single vehicle, such as headway and free speed, and also their connection with the macroscopic traffic indices, such as platoon size and delay, was analyzed (2, 3). In this context, the stochasticity was mainly considered to be the same as the heterogeneity among drivers. In other words, it was assumed that the desired speed and headway distance of each vehicle is given by “rolling a dice” according to a predefined probability distribution, as is commonly employed in conventional traffic flow simulations. As a result of “rolling a dice,” the traffic flow

represented in the simulations can yield a variety of results with some probability.

In the last decades, stochasticity has been examined in conjunction with traffic dynamics, in which stochastic characteristics are often introduced into a model as additional variables following a specific form of a probability distribution. For instance, Laval et al. showed that the formation and propagation of traffic oscillation can be explained by adding a white noise to drivers' desired acceleration in free-flow (4). Treiber and Kesting examined an external acceleration noise on the car-following models (5). While these studies indicate that the

¹Ritsumeikan University, Kusatsu, Japan

²TU Delft, Delft, the Netherlands

Corresponding Author:

Yasuhiro Shiomi, shiomi@fc.ritsumeik.ac.jp

stochasticity plays an important role in representing traffic dynamics, given the conjecture raised by Chen et al., Tian et al., and Xu and Laval that car-following behavior of a driver consists of several regimes, it is not sufficient to assume a uniform distribution form for the noise term regardless of traffic state (6–8). In line with this conjecture, Yuan et al. show that the standard deviation (SD) of a driver's desired acceleration linearly decreases as their speed increases and, based on this, they proposed an extended parsimonious car-following model which can represent capacity drop (9). The Cox-Ingersoll-Ross process was used by Ngoduy et al. to develop a stochastic car-following model that describes the time-varying random acceleration and theoretically deduces the impact of the random parameter on traffic instabilities (10). The same approach is applied to higher order continuum traffic models (11). Xu and Laval generalize the Brownian and geometric Brownian acceleration processes in two-regime car-following models (4, 8, 9). They reveal that the estimated parameters are consistent within the same dataset but different across datasets, according to the results of parameter calibration using experimental data. Additionally, they find that the acceleration error process is close to a Brownian motion.

These studies are successful in capturing the stochasticity and heterogeneity of acceleration behaviors, but they do still assume that the stochastic terms follow a Gaussian distribution for the sake of mathematical tractability and pay less attention to the shape of the stochastic terms and, instead, assume a Gaussian distribution. Furthermore, stochasticity is composed of the random error of driving behavior caused by lack of perception, error of operations, and so on, as well as the heterogeneity, but the randomness and the heterogeneity are not explicitly distinguished in the previous studies. When significant acceleration or deceleration is required, the distribution's shape can be asymmetric because the performance of vehicles limits the maximum acceleration and deceleration. In addition, the distribution shape is not necessarily unimodal but can be multimodal, given that the stochastic term in acceleration takes into account heterogeneity in driving behavior (12–14). This is easily imagined by thinking about the differences between a timid and an aggressive driver. In a separate line of research on heterogeneity, Fadhloun et al. developed a vehicle-dynamics-based acceleration model that explicitly incorporates differences in the gas-pedal operation by drivers (15). Makridis et al. proposed a free-flow acceleration model that incorporates various gear-shifting strategies and driving styles with vehicle dynamics. However, they are limited to free driving conditions (16).

The difficulty in assuming non-Gaussian distribution for the random term is that it cannot be observed. In recent years, however, large amounts of vehicle

trajectory data on freeways (e.g., Krajewski et al. and Seo et al.) have been publicly available (17, 18). These data make it possible to create a model that predicts driving behaviors using a data-driven methodology. For instance, Gilles et al. propose a framework for addressing the motion forecasting problem that outputs an image that depicts the probability distribution of the agent's future location (19). The data-driven approaches using trajectory datasets also have drawn much research attention for modeling driving behaviors. Zhou et al. proposed a microscopic car-following model based on recurrent neural network to detect and predict traffic oscillation (20). Fan et al. and Wang et al. applied a long short-term memory (LSTM) neural network to a car-following model, demonstrating the significance of the long memory (21, 22). Lee et al. integrate the stochastic car-following model and neural-network-based lane-changing model and find that the proposed model can tackle the unpredictable fluctuations in the velocity of the vehicles in the acceleration/deceleration zone (23). Using LSTM, Zhang et al. develop a unified model of car-following and lane-changing and demonstrate that the model can successfully predict the occurrence of lane-changes (24).

To the best of the authors' knowledge, these models are deterministic and fail to take into account the stochastic nature of traffic flow, although data-driven modeling of driving behavior is promising with regard to its capability to capture driving behavior and represent traffic dynamics. To fill this gap, we develop an LSTM-based car-following model that predicts the probabilistic distribution of the acceleration. The acceleration values to be trained are discretized into bins, and the model predicts the probability that the acceleration for the next time step will be in a bin. This enables the model to produce a non-parametric acceleration distribution. After assessing the accuracy of the proposed model using data on vehicle trajectory collected on a freeway in Japan, the statistics of mean, SD, asymmetry, and distribution modality are looked at in relation to traffic conditions. We also showed that heterogeneity in driving behavior can be expressed as the time-series variation of percentiles of the realized values relative to the distribution.

The remainder of this paper is organized as follows. The modeling framework is described in the following section. The data used in the study are presented in the section that follows that, after which the results of the training and assessment of the prediction accuracy are discussed. The statistical characteristics of the stochastic terms and the traffic conditions are then compared, and the heterogeneity of driving behaviors based on realized acceleration values is also examined. Finally, the results obtained are summarized and suggestions for future research are made.

Model Specification

The acceleration of vehicles is the result of each driver's sequential operation of the accelerator pedal in response to the surrounding environment, their own state, and the current traffic conditions. It is necessary to take spatio-temporal factors into account when modeling the accelerating and decelerating behavior of vehicles. Furthermore, since the driver's perception and operation involve some degree of error, the model should depict the stochasticity of the behavior of the vehicle. In this section, we describe the details of a model using LSTM.

Architecture of LSTM

This study adopts the principle formulation of Ngoduy et al. to predict the target vehicle's acceleration and deceleration in relation to the environment, including the traffic state and road geometry shown by Equation 1 (10):

$$dv_i(t) = f(\Theta_i(t))dt + g(\Theta_i(t))dt \quad (1)$$

where

$v_i(t)$ = the speed of vehicle i at time t ,

$\Theta_i(t)$ = the state variables of vehicle i until time t ,

$f(\cdot)$ = a function returning a deterministic acceleration value, and

$g(\cdot)$ = a function returning a stochastic source depending on $\Theta_i(t)$.

Equation 1 is distinct from Ngoduy et al. in the point that the stochastic term, $g(\cdot)$, is assumed to be determined by the state variable $\Theta_i(t)$, which can include any factors affecting vehicle behaviors such as the driving state of a target vehicle, the interactions with surrounding vehicles, road geometric features, attributes of a target vehicle, and so on (10). In this study, instead of defining an explicit formulation for $f(\cdot)$ and $g(\cdot)$, they are expressed by a data-driven model. More specifically, the model makes use of LSTM, the ability of which to reproduce car-following behaviors has been demonstrated in earlier studies (21, 22).

The LSTM approach has a long-term memory in which unimportant information in the training data can be discarded. To address the vanishing gradient issue in recurrent neural networks, a hidden layer of LSTM incorporates forget gates, input gates, memory cells, and output gates. For the details of LSTM, we refer to Hochreiter and Schmidhuber (25). Figure 1 depicts the schematic representation of an LSTM structure. In this figure, ς , τ , and σ denote activation functions. $\mathbf{h}(t)$, $\mathbf{c}(t)$, $\mathbf{y}(t)$, $\mathbf{f}(t)$, $\mathbf{i}(t)$, $\mathbf{a}(t)$, and $\mathbf{o}(t)$ denote the vector of a hidden layer, the vector of a memory cell, the vector returned from the forget gate, the vector returned from the input gate, the vector of the current hidden state values activated by ς and τ , and the vector returned from the output gate, respectively. Each vector is written as Equations 2 to 8:

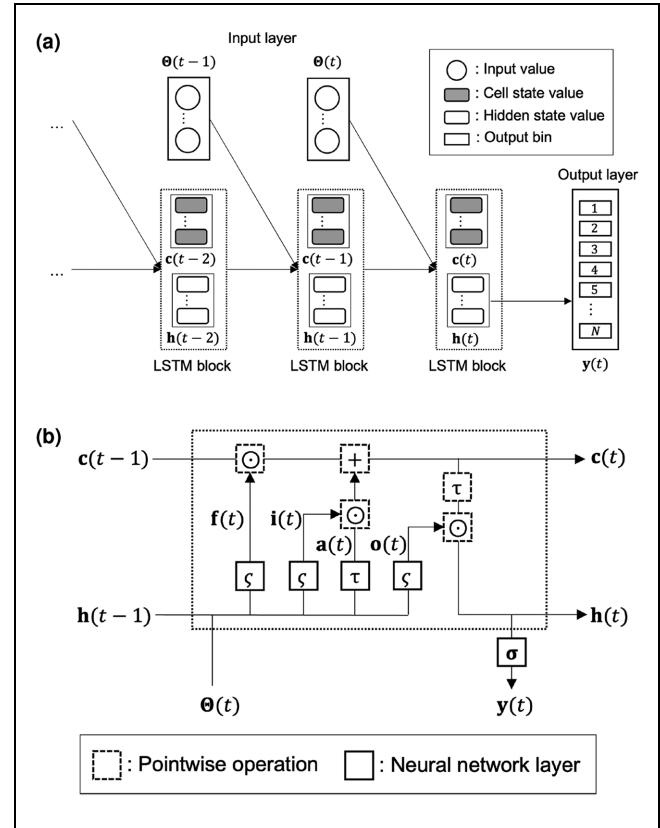


Figure 1. A schematic of long short-term memory (LSTM) network: (a) whole structure of LSTM network and (b) structure of LSTM block.

$$\mathbf{f}(t) = \varsigma(\Theta(t) \cdot \mathbf{U}^f + \mathbf{h}(t-1) \cdot \mathbf{W}^f) \quad (2)$$

$$\mathbf{i}(t) = \varsigma(\Theta(t) \cdot \mathbf{U}^i + \mathbf{h}(t-1) \cdot \mathbf{W}^i) \quad (3)$$

$$\mathbf{a}(t) = \tau(\Theta(t) \cdot \mathbf{U}^a + \mathbf{h}(t-1) \cdot \mathbf{W}^a) \quad (4)$$

$$\mathbf{o}(t) = \varsigma(\Theta(t) \cdot \mathbf{U}^o + \mathbf{h}(t-1) \cdot \mathbf{W}^o) \quad (5)$$

$$\mathbf{c}(t) = \mathbf{f}(t) \odot \mathbf{c}(t-1) + \mathbf{i}(t) \odot \mathbf{a}(t) \quad (6)$$

$$\mathbf{h}(t) = \mathbf{o}(t) \cdot \tau(\mathbf{c}(t)) \quad (7)$$

$$\mathbf{y}(t) = \sigma(\mathbf{h}(t) \cdot \mathbf{V} + \xi) \quad (8)$$

where

\mathbf{U} = coefficient vector,

\mathbf{W} = coefficient vector,

\mathbf{V} = coefficient vector,

ξ = the biases, and

\odot = the Hadamard product.

The sigmoid function and the hyperbolic tangent function applied to the activation functions, ς and τ .

Although the observed value of acceleration is initially continuous, the entire range of acceleration is divided into N bins to predict the non-parametric probability distribution of the acceleration. Then, the model is set up to

output the probability that an observation value, $y_i^{obs}(t)$, falls into each bin. Thus, the softmax function is applied to $\sigma(\cdot)$ which is written by Equations 9 and 10:

$$\sigma(\mathbf{z}) = (\sigma_1(\mathbf{z}), \dots, \sigma_N(\mathbf{z})) \quad (9)$$

$$\sigma_i(\mathbf{z}) = \frac{\exp(z_i)}{\sum_j^N \exp(z_j)}, \quad i \in \{1, \dots, N\} \quad (10)$$

Loss Function

It is critical to predict strong acceleration/deceleration behavior when modeling traffic dynamics, but these behaviors are rarely observed when compared with stable conditions. As a result, we need to pay relatively more attention to these rare cases in training. In this study, we use focal loss (FL) as a loss function to be minimized, which allows us to handle the class imbalance naturally without undersampling (26). FL is an extension of the cross entropy (CE) loss. It down-weights the dominant classes with a high probability of classification, allowing training to be focused on rare classes. To accomplish this, a modulating term is added to the CE loss, which reduces the loss value relatively if its probability is high.

Suppose p_i denotes the estimated probability of class i and y denotes the ground-truth class, and define p_i^t as:

$$p_i^t = \begin{cases} p_i & (i = y) \\ 1 - p_i & (otherwise) \end{cases} \quad (11)$$

the CE can be written as Equation 12:

$$CE(p_i^t) = - \sum_{i=1}^N \ln(p_i^t) \quad (12)$$

In FL, a modulating factor $(1 - p_i^t)^\gamma$ is added to CE with an adjustable parameter $\gamma \geq 0$. FL is defined by Equation 13:

$$FL(p_i^t) = - \sum_{i=1}^N \alpha^t (1 - p_i^t)^\gamma \ln(p_i^t), \quad (13)$$

where

α^t = a weighting factor and defined with a parameter $\alpha \in [0, 1]$ as follows:

$$\alpha^t = \begin{cases} \alpha & (i = y) \\ 1 - \alpha & (otherwise). \end{cases} \quad (14)$$

Figure 2 shows the relationship between the probability and the loss values given by Equation 13, in which α^t is fixed to 1. It is intuitively obvious that, as the probability near 1.0 and γ increases, the modulating term becomes 0 and the loss values for the well-classified class can be down-weighted.

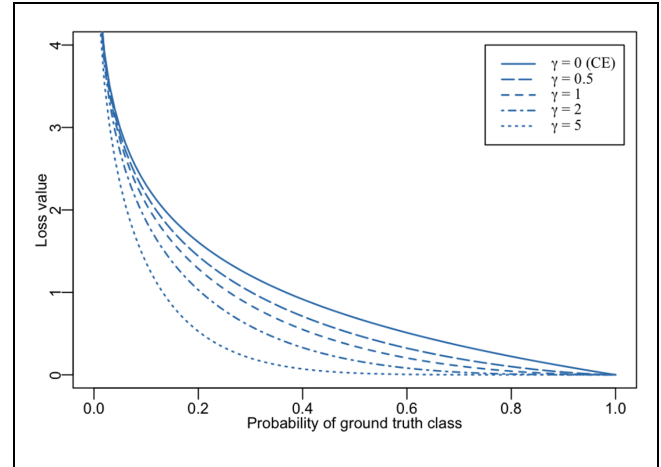


Figure 2. Focal loss (FL) function (26).

Note: CE = cross entropy.

Input and Output Variables

Although the use of LSTM allows us to consider the time-series effects of car-following behavior, more input variables are required to capture the spatial characteristics of traffic dynamics. As a result, we consider the anticipation effect as well as the spatial propagation of stop-and-go waves using the speed, acceleration, headway distance, and relative speed with multiple leading vehicles as input variables (27). The headway distance of i th vehicle to n vehicles ahead, $\Delta x_i^n(t)$, is defined as $x_{i+n}(t) - x_i(t)$ where $x_i(t)$ shows the position (m) of vehicle i at time instant t , and the relative speed of i th vehicle with n vehicles ahead, $\Delta v_i^n(t)$, is defined as $v_{i+n}(t) - v_i(t)$ where $v_i(t)$ shows the speed of vehicle i at time instant t . In addition to the effect of leading vehicles, the effect of following vehicles is taken into account as an input variable to capture the influence of being tailgated (28). This is represented by setting n to a negative integer.

Concerning the attribution of each vehicle, a vehicle length (m) and a type of vehicle (0: passenger car and 1: truck) are included both for a target vehicle and its surrounding vehicles. The holiday dummy (1: the data is observed on holiday, 1: otherwise) and morning dummy (1: the data is observed in the morning peak, 0: otherwise) are also used as the input variables. This is because, as suggested by Lenné et al., Yeon et al., and others, drivers' driving characteristics may differ depending on the time of day (29, 30).

Both gradient and turning radius are considered as factors of road geometric features which influence vehicle behavior. More specifically, the average of gradient from $x_i(t) - 50$ m to $x_i(t) + 50$ m is used for smoothing the gradient effect, and the curvature radius at 50 m ahead is used as an input variable, since drivers would adjust their speed before reaching the location of the

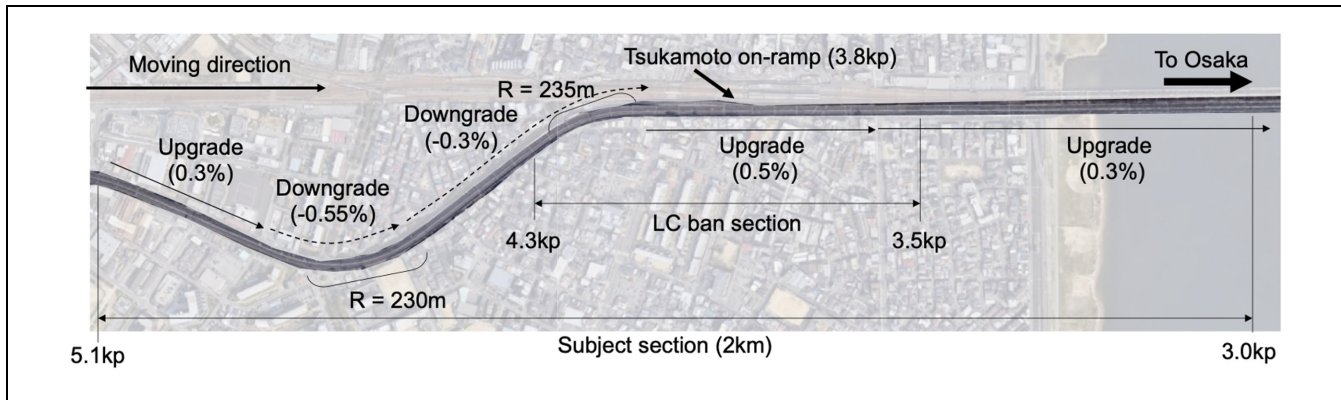


Figure 3. Overview of the subject section.

Note: LC ban = lane change banned.

Table 1. Sample Size of Datasets

No.	Time and day	No. of unique vehicle ID	No. of records
1	7:00–8:00 on weekday	2,164	3,169,367
2	15:00–16:00 on weekday	2,121	2,258,147
3	10:00–11:00 on holiday	1,898	2,515,658
4	7:00–8:00 on weekday	2,225	3,188,724
5	15:00–16:00 on weekday	1,998	2,329,178

minimum curvature radius to keep their safety and comfort. It should be noted that, because this study focuses on longitudinal driving behavior, the impact of adjacent lanes (e.g., discussed by Ponnu and Coifman) is ignored (31). Although this is a subject for future work, this proposed modeling framework can naturally take account of the influence of adjacent lanes by including features of traffic states on the adjacent lanes, and the model can even be easily extended to represent the integration of car-following and lane-changing.

The acceleration of the target vehicle after a one-time step is set as an output variable. Because LSTM can account for time-series variation including the influence of the reaction delay, the model does not explicitly consider reaction delay time as a parameter.

Data

In this study, we use vehicle trajectory data for model training and validation. This section provides an overview of the data to be used and its preprocessing method.

Trajectory Dataset

To develop a robust model using a data-driven approach, it is necessary to use data that cover the vehicle maneuvers in various traffic states including free-flow state, as well as the generation and propagation of stop-and-go

waves. We use Zen Traffic Data (ZTD) provided by Hanshin Expressway Co. Ltd. in Japan (18). ZTD utilizes an image sensing technology to create data on the position and speed of each vehicle driving in the target section in 0.1 s increments. The overview of the subject section is shown in Figure 3. It is located approximately 5 km from the center of Osaka City on Route 11 Ikeda Line and is a two-lane section bounding for the center of Osaka City consisting of an up-and-down gradient section, a sharp curve section, a merge section from an on-ramp, and a lane change banned (LC ban) section. Because this paper focuses on car-following behavior, the data from the median lane is only used for this analysis.

The data collection was done on different 5 days for each 1 h. As a result, we have 5 h data in total. The sample sizes of the dataset are shown in Table 1. The precise date of the data collection is concealed. Figure 4 depicts the time-space diagram of dataset No. 4 as an example to see the traffic flow characteristics in the target section. It is clear that the stop-and-go waves are generated within the LC ban section and propagate upstream.

Preprocessing

The original data in ZTD was collected by video cameras. Because of the limited distance that one camera can cover, the trajectories collected by each camera must be combined to generate the trajectories in the 2 km stretch

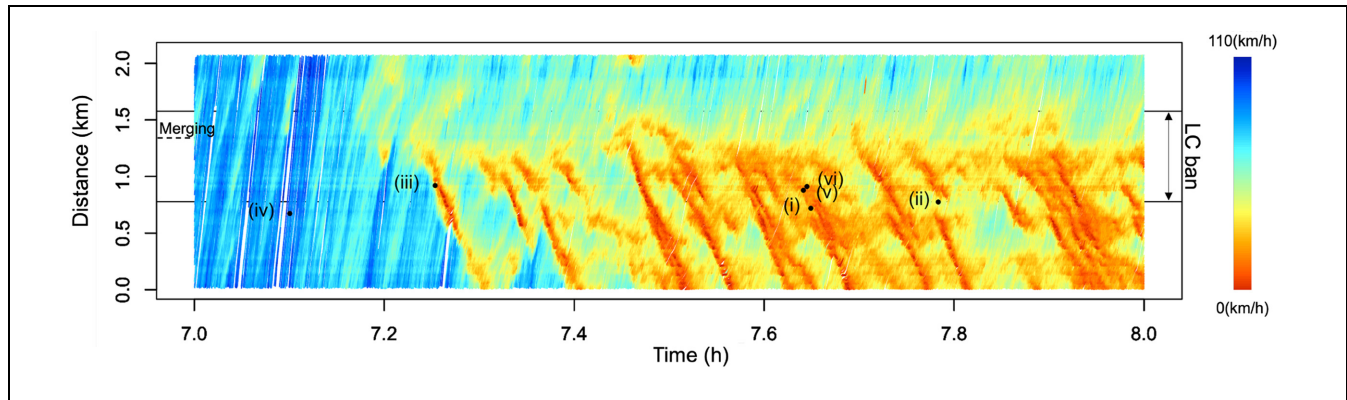


Figure 4. Time-space diagram in dataset No. 4.

Note: (i) = prediction result at (time, distance) (7.6492, 0.7190); (ii) = at (7.7833, 0.7753); (iii) = at (7.2536, 0.9200); (iv) = at (7.1006, 0.6733); (v) = at (7.6413, 0.8780), and (vi) = at (7.6450, 0.9115); LC ban = lane change banned.

section. As a result, it may contain some systematic errors. To eliminate these errors, the sequence of the speed for each trajectory is smoothed by taking a moving average of 1 s before and after, which corresponds to 20 data points. A moving average ensures that the speed integration after smoothing is consistent with regard to the actual distance to travel. Subsequently, the acceleration value $a(t)$ to be predicted with the input variables at time t is defined as:

$$a(t) = \frac{dv(t)}{dt} := \frac{v(t + \Delta t) - v(t)}{\Delta t} \quad (15)$$

where

Δt = the incremental size of time and set to 0.1 s in this study.

However, some outliers remain, so extreme cases where the absolute value of the acceleration is greater than 10 km/h/s, which corresponds to less than 0.01% of the total data, are discarded.

Model Performance

Settings

To apply the proposed model, according to the results of the sensitivity analysis we did before the training, the number of vehicles considered as input variables representing the spatial and anticipation effect is set as three vehicles ahead and one vehicle back, that is, $n = \{-1, 1, 2, 3\}$. Then, all variables are normalized to $[0, 1]$ by min-max feature scaling denoted by Equation 16.

$$\tilde{x} = \frac{x - x_{min}}{x_{max} - x_{min}}, \quad (16)$$

The size of bins in the output layer is set as 1,000, meaning that the acceleration value to be predicted is discretized to each 0.02 km/h/s, since the acceleration range is

limited from -10 km/h/s to 10 km/h/s. This is also normalized by min-max feature scaling.

In the case of LSTM, the lookback period is set to 50, indicating that the data from 5 s ago to now is used for the prediction. The other hyperparameters and the settings of LSTM are defined based on the preliminary survey as follows: the input dimension is 28; batch size is 512; the number of hidden layers of LSTM is 32; optimizer is Adam; learning rate is scheduled with initial learning rate, 0.01, decay rate, 0.9, and decay steps, 10,000; γ and α of FL (Equation 13) are 2.0 and 0.25, respectively. In total, the number of parameters to be trained is 41,225.

All trajectories are randomly divided into 80% for training and validation and 20% for testing. The former is further subdivided into 80% for training and 20% for validation. To avoid overfitting, a non-overlapping sliding window is used for training and validation. As a result, 175,958 samples are used for training and validation, and 43,603 samples are used for testing. The model was developed with the Keras deep learning library and the TensorFlow backend.

A Benchmark Model

Besides the LSTM-based model we proposed, we calibrate an extended Helly model as a benchmark (27). The model formulation is denoted by Equation 17:

$$a(t) = \sum_{j=1}^{m_1} \alpha_j \Delta v_j(t - \tau) + \sum_{j=1}^{m_2} \beta_j (\Delta x_j(t - \tau) - S_j) \quad (17)$$

where

m_1 and m_2 = the number of leaders to which a driver responds,

τ = the reaction delay,

Δv_j = relative speed with j th vehicle ahead,

Δx_j = gross distance between both vehicles,

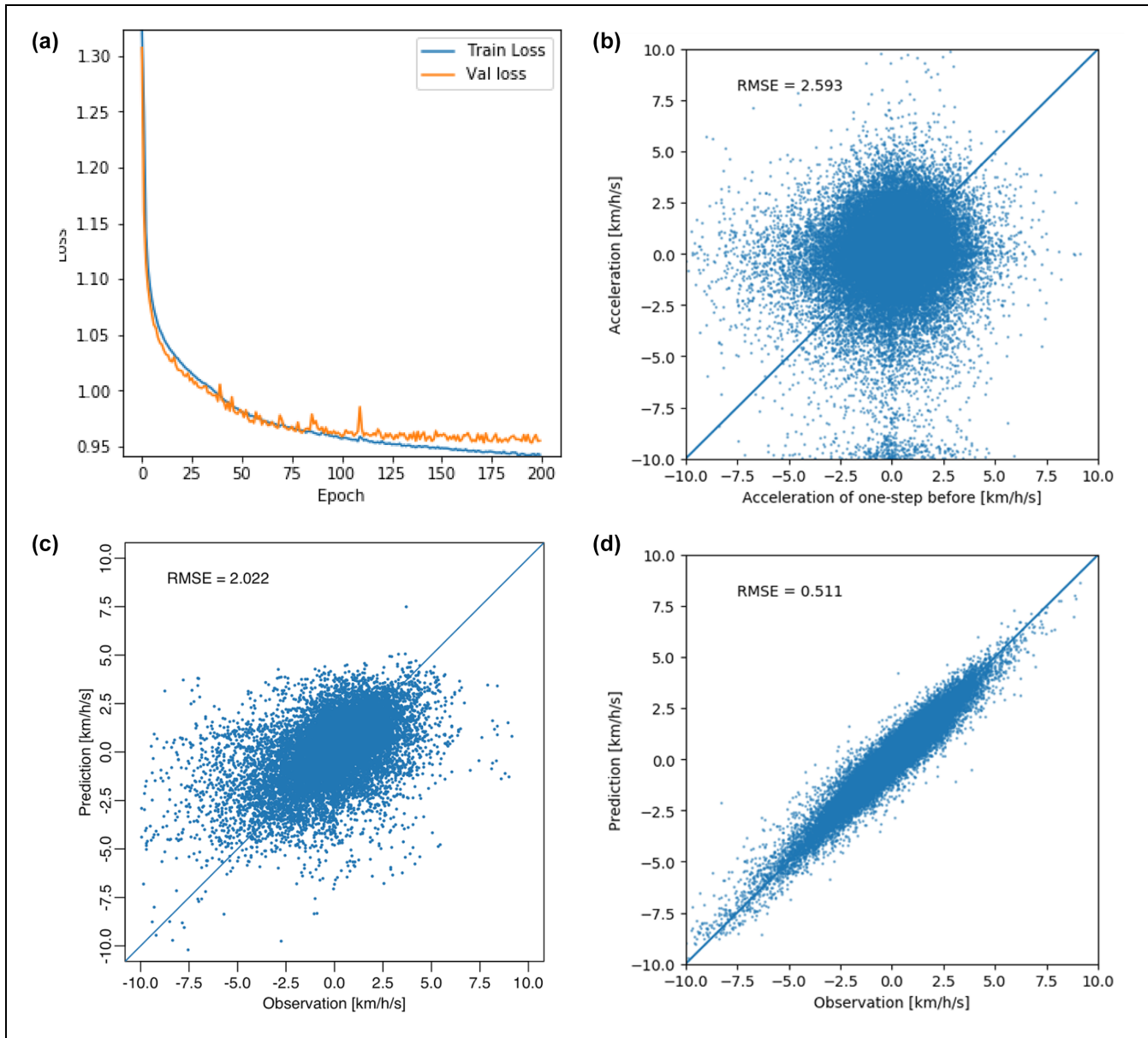


Figure 5. Comparison between ground truth and prediction: (a) loss plot, (b) one time step before, (c) Helly model, and (d) long short-term memory (LSTM) model.

Note: RMSE = root mean square error.

S_j = desired distance to j th vehicle ahead, and α_j and β_j = sensitivity parameters.

We set $m_1 = m_2 \in \{1, 2, 3\}$ and $0.5 \leq \tau \leq 3.0$. Then, such m_1 , m_2 , and τ that provide the highest adjusted coefficient of determination (R_{adj}^2) are estimated trajectory by trajectory. 80% of data in a trajectory is randomly chosen for estimating the parameters and the other 20% is used for testing the prediction accuracy. If R_{adj}^2 is less than 0.60, its driving behavior is considered to be inconsistent with the assumptions of the Helly model and not used for the further evaluation.

Results

The results of training, validation, and testing are summarized in Figure 5. Figure 5a depicts the loss values sequence at each epoch during the training process. The model is well converged and the difference between training loss and validation loss is small, implying that the model can avoid over-fitting. Figure 5, b to d, compares the relationship between the ground truth and the prediction for test dataset among three methods—Figure 5b: acceleration values at one time step (0.1 s) before; Figure 5c: the Helly model described above; and Figure 5d: the

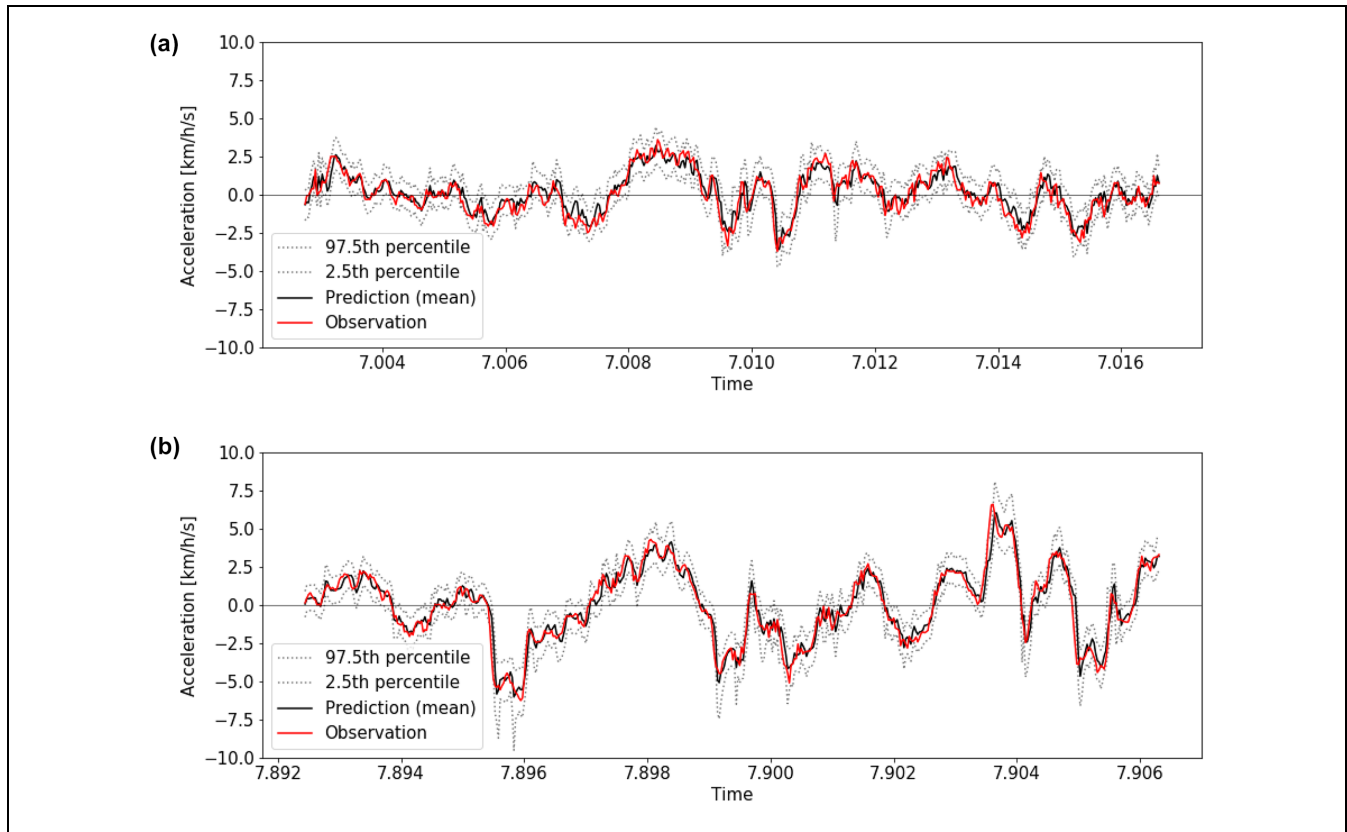


Figure 6. Model prediction versus observation with 95% confidence interval: (a) in free-flow and (b) in congestion.

LSTM model proposed in this study. In this case, the arithmetic mean of the predicted distribution is used because the LSTM model predicts the distribution of the acceleration. Figure 5b demonstrates that the serial correlation of the acceleration sequence is not visible. The extended Helly model cannot predict the acceleration well, especially when strong acceleration and deceleration are needed, according to Figure 5c. On the other hand, the LSTM model can offer extremely accurate predictions across the entire acceleration range. Trajectory by trajectory, the Helly model's parameters are calibrated. Nevertheless, the prediction's precision is modest. This is because the Helly model assumes a linear relationship between the stimuli a driver receives and the driver's acceleration behavior and does not capture the time-series effect. High-quality predictions are made possible by the LSTM's relaxation of these presumptions and accounting for time-series variations.

Then, using the trained LSTM model, we simulated the trajectory of a few particular vehicles. Figure 6 depicts the mean of predicted acceleration, the observed acceleration values, and a 95% confidence interval for a particular vehicle (upper bound is 97.5th percentile value and lower bound is 2.5th percentile value). Figure 6a is an example of a trajectory in the free-flow state and

Figure 6b is in the congestion state. As can be seen, the prediction closely matches the observation, and, in the majority of cases, the observation falls within the confidence interval regardless of the traffic conditions or even circumstances requiring significant deceleration and acceleration. It is also remarkable that the width of the confidence interval varies depending on the situation. In a free-flow situation, the interval is mostly within ± 1.0 km/h/s, while in the congested case it becomes larger than ± 2.5 km/h/s when the time is 7.896 in Figure 6b, for example. This suggests that driving behavior's stochastic traits alter in response to traffic conditions. Also, take note that the range of the confidence intervals' range is much smaller than what Ngoduy et al. presented (10). This might be because the model can capture the characteristics of acceleration and deceleration behavior and, as a result, the accuracy of the deterministic term becomes higher.

Analysis of Stochasticity

When the estimated probability distribution follows a normal distribution, it is assumed that randomness is primarily to blame for the acceleration variation. On the other hand, if the probability distribution is multimodal,

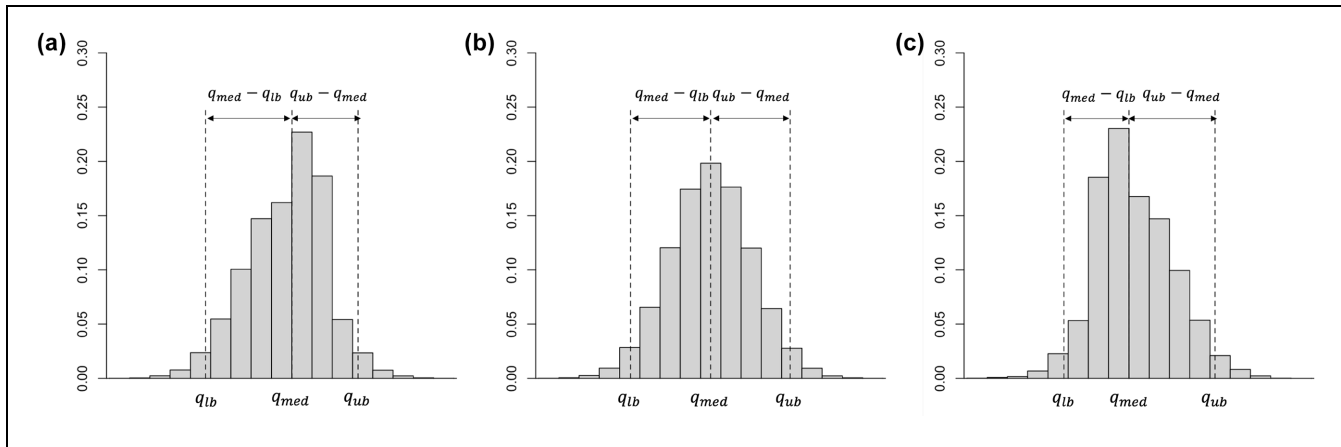


Figure 7. Examples of the degree of asymmetry (I_A): (a) $I_A < 0$, (b) $I_A = 0$, and (c) $I_A > 0$.

then several different acceleration and deceleration behaviors are expected, which may diverge in the subsequent traffic conditions. It would be beneficial to comprehend the nature of traffic dynamics if there were any relationship between multimodality and traffic state. This section focuses on the shape of the acceleration distribution. Before analyzing the relationship between the shape of the acceleration distribution and traffic state, we first introduce the metrics related to the distribution's shape, namely the SD, modality, and degree of asymmetry (I_A).

Metrics of Stochasticity

SD, modality, and I_A are used as metrics to assess the shape of the predicted acceleration distribution. To identify multimodality in this study, we apply the dip test among several methods, since it is a non-parametric method and does not require a specific kernel function (32). The dip test measures multimodality (or non-unimodality) in each sample over all sample points by the maximum difference between the observed distribution function and the unimodal distribution function that minimizes that maximum difference. The procedure of the dip test is as follows. First, randomly generate n variables that follow the estimated probability distribution to be tested, and denote them as $\mathbf{x} = \{x_1, \dots, x_n\}$ in ascending order, and its empirical cumulative frequency distribution is denoted by F_n . Choose any pair of $(x_i, x_j)_{i < j}$ and compute the greatest convex minorant of F_n in the interval $(-\infty, x_i)$ and the least concave majorant of F_n in the interval (x_j, ∞) . d_{ij} denotes the maximum distance between these two curves and F_n . Then, twice the minimum value of d_{ij} for the possible combination of (i, j) is defined as a "dip" statistic. The probability distribution's unimodality is statistically rejected if this dip statistic exceeds a predetermined threshold value, as shown in

Hartigan and Hartigan (32). For more details on the computational algorithm, we refer to Hartigan (33).

Concerning I_A , we evaluate it by Equation 18 instead of the skewness, since the distribution can be multimodal:

$$I_A = (q_{ub} - q_{med}) - (q_{med} - q_{lb}) \quad (18)$$

where

$$\begin{aligned} q_{ub} &= 97.5 \text{ percentile value,} \\ q_{med} &= \text{the median, and} \\ q_{lb} &= 2.5 \text{ percentile value.} \end{aligned}$$

Figure 7 shows examples of the shape of distribution and its corresponding I_A to help comprehend this index of asymmetry. As shown in Figure 7, if $I_A < 0$, the tail of the large acceleration is long, and vice versa.

Traffic State and Stochasticity

We examine the relationship between traffic state and the shape of acceleration distribution. Its shape is evaluated by unimodality, SD, and I_A .

Visualization of SD and Multimodality. The proposed model is applied to the dataset No. 4 shown in Table 1. Every 1 s, the entire trajectory and its acceleration distributions are predicted. In Figure 8, where the bandwidth of kernel density estimation is set as 15, six examples of the shape of the kernel density distribution of predicted acceleration are displayed. In the figure, the distribution (i) corresponds to a prediction result at (time, distance) = (7.6492, 0.7190) of Figure 4. Likewise, the distribution (ii) is at (7.7833, 0.7753), the distribution (iii) is at (7.2536, 0.9200), the distribution (iv) is at (7.1006, 0.6733), the distribution (v) is at (7.6413, 0.8780), and the distribution (vi) is at (7.6450, 0.9115). Each distribution's variance and asymmetry differ depending on how

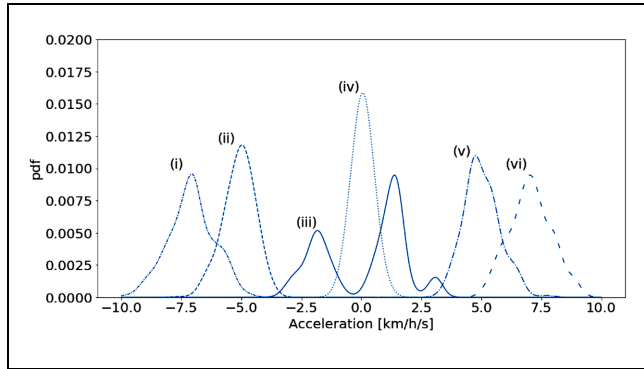


Figure 8. Examples of the distributions (i) to (vi) of the predicted acceleration.

Note: (i) = prediction result at (time, distance) (7.6492, 0.7190); (ii) = at (7.7833, 0.7753); (iii) = at (7.2536, 0.9200); (iv) = at (7.1006, 0.6733); (v) = at (7.6413, 0.8780), and (vi) = at (7.6450, 0.9115).

strongly an object accelerates or decelerates. It should be also noted that distribution (iii) has a tri-modal shape, implying that driver's reaction at this time and place is likely to diverge.

Figure 9a displays the measured trajectories colored according to the predicted SD of the acceleration, and Figure 9, b and c, displays magnified views of particular time-space regions to help understand the overall tendency. Each dot in Figure Figure 9, a to c, depicts the moments where the unimodality of the estimated distribution is rejected at a significance level of 5% by the dip test.

We can see in Figure 9a that the SDs just the downstream of the LC ban (indicated as a box [a] in the figure) section are higher than the other section. This tendency is clear, particularly in the free-flow state before the time is 7.25. This is because of the likelihood of lane changes from the outside lane to the median lane to avoid conflicts with the merging vehicles, which may cause a vehicle on the median lane to decide to accept the lane-changers or not. Additionally, it can be seen that the SDs tend to be high at the upstream and downstream edge of the stop-and-go wave. This suggests that situations requiring rapid acceleration and deceleration tend to have higher levels of driving behavior variability.

Concerning the modality, 426 cases in 261,540 are found to be multimodal, and they are mainly distributed along with the stop-and-go waves. This tendency is clearly confirmed in the magnified views shown in the figures. Figure 9b is a magnified view of the region where the first stop-and-go wave is generated. This figure demonstrates that the SDs tend to be higher before the speed reduction occurs and that multimodality is present near the origin of the stop-and-go wave. Figure 9c is the case that the stop-and-go wave was propagated from the the downstream section. It demonstrates a nearly

identical trend to Figure 9b, namely that the SDs increase before and after the speed reduction. It makes sense that drivers do not have a wide range of options when forced to follow a leading vehicle at a low speed, but during the phase of deceleration and acceleration, they can adjust the amount of deceleration and acceleration and may also have the opportunity to change lanes, causing reaction behavior to diverge and fluctuate. It may affect the traffic dynamics such as capacity drop and oscillation.

Aggregation Analysis. Each metric of the predicted distribution is examined collectively to see the characteristics of the distribution's shape. Figure 10a depicts the relationship between the speed and the SD of acceleration distribution and between the speed and the asymmetry of acceleration distribution in 5 km/h speed bins. Note that it is limited to the cases where the acceleration is larger than 0. As speed increases, it can be seen that the SD of acceleration decreases, indicating that, after a significant speed reduction, the accelerating behavior tends to diverge and fluctuate. This finding supports the assertion of Yuan et al. that the decreasing trend of SD as the speed increases is an essential factor to represent traffic dynamics (9). Regardless of the speed level, asymmetry has a positive mean. The positive I_A means that the distribution has a long tail toward the higher acceleration. This figure is depicted using the data when vehicles need to accelerate, and the probability that the acceleration value becomes negative in such a situation is extremely low, therefore, the distribution would be censored in the negative direction. On the other hand, the drivers can take their own desired acceleration unless the vehicle catches up with the vehicle in front. The distribution has a long tail in a positive direction because of this. When the vehicle is moving at a speed slower than 10 km/h, this tendency becomes more obvious.

Figure 10b summarizes the relationship between the mean of acceleration and the mean of SD and between the mean of acceleration and the mean of the I_A in 2.5 km/h acceleration bins. As can be seen, the SD is the lowest when the mean acceleration is almost zero, but it rises as the absolute value of the mean increases. This result is in line with the above findings that the SDs become higher at the generation of stop-and-go waves where speed disturbances occur and before and after the stop-and-go waves where strong deceleration and acceleration are required. Concerning asymmetry, the shape of acceleration distribution is nearly symmetric when the mean of acceleration is close to zero. As the mean acceleration increases (decreases) the I_A becomes increases (decreases) until 5.0 km/h/s (-5.0 km/h/s), then decreases (increases). When the acceleration is lower than 5.0 km/h/s, the tail of higher acceleration becomes

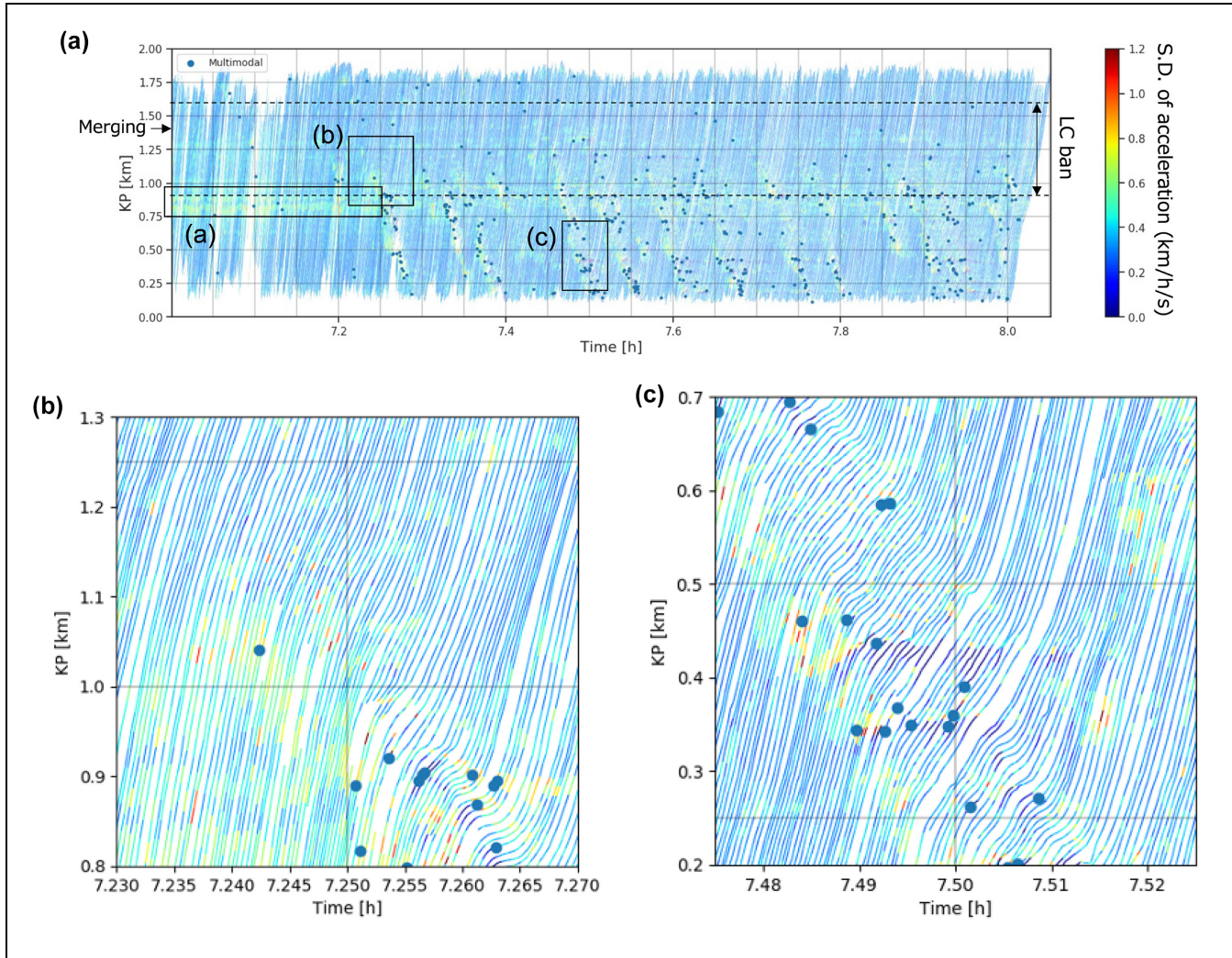


Figure 9. Standard deviation (SD) and multimodality of acceleration distribution: (a) measured trajectories colored according to the predicted SD of the acceleration, (b) time-space region (b), and (c) time-space region (c).
 Note: KP = kilopost; LC ban = lane change banned.

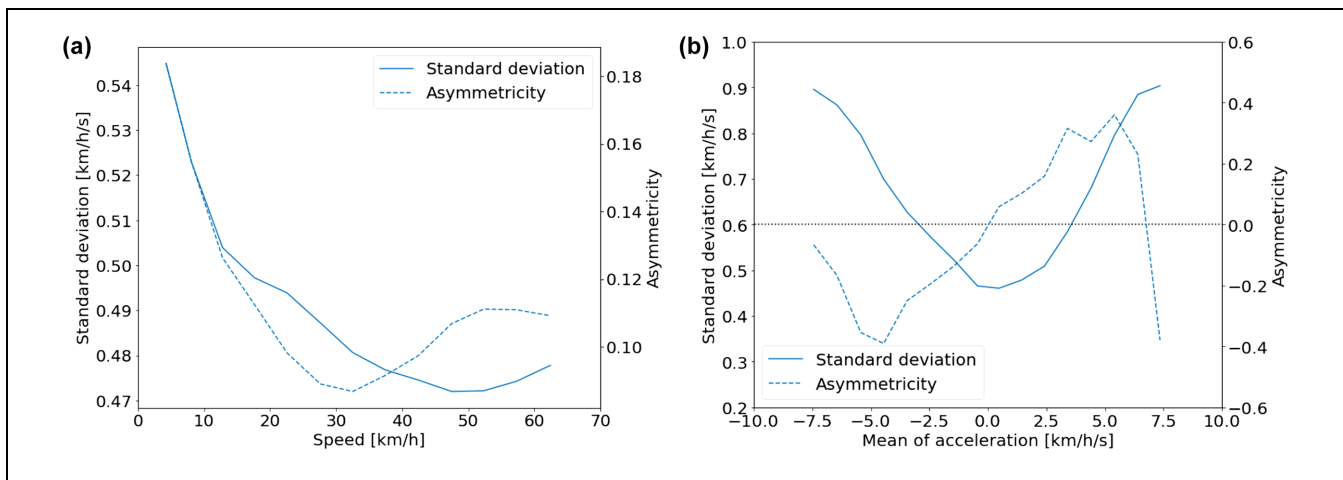


Figure 10. Relationship among metrics of acceleration distribution: (a) speed, standard deviation (SD) and asymmetry and (b) mean, SD, and asymmetry.

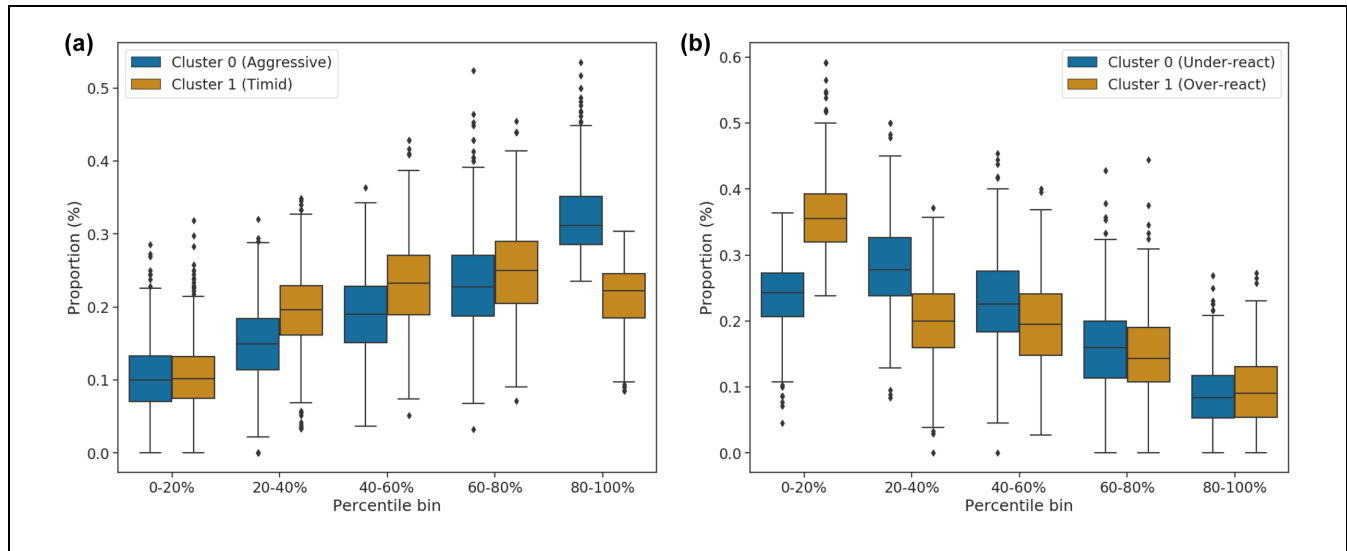


Figure 11. Box plots of each cluster: (a) acceleration phase and (b) deceleration phase.

long because of the same reason mentioned about Figure 10a. However, when the acceleration is higher than 5.0 km/h/s, the highest acceleration is bounded because of the performance of vehicles. Because of this, the I_A becomes negative. In the case of deceleration, the distribution shape is long-tailed in the negative direction when the mean acceleration is greater than -5.0 km/h/s. However, in traffic situations where strong deceleration is necessary, the maximum deceleration is constrained by the vehicle performance, so the distribution shape approaches symmetry. These findings imply that the shape of the stochastic term in Equation 1 does not always conform to the normal distribution but can instead change depending on the traffic situation.

Analysis of Heterogeneity

The previous section revealed that the shape of the distribution of acceleration which is predicted by the proposed data-driven car-following model varies depending on its driving speed and acceleration. However, it is considered that the stochasticity of the acceleration consists of both intra-vehicle heterogeneity and inter-vehicle variations in driving behavior, which are not explicitly separated. This section focuses on time-series variations in the relationship between the predicted acceleration distribution and the drivers' actual acceleration and demonstrates how this model can account for driver heterogeneity.

Methodology

Suppose drivers can be classified into several patterns according to their driving characteristics. In the acceleration phase, drivers can be classified into timid and

aggressive (34). The former may often carry out lower acceleration, while the latter may often carry out higher acceleration. In the deceleration phase, they can be classified into under-react and over-react (35). The former may often carry out weak deceleration, while the latter may often carry out strong deceleration. As a result, one measure of the heterogeneity of driving behavior is the sequence pattern of the percentiles of the acceleration that the driver carries out relative to the predicted distribution.

Therefore, we calculate the percentile values of the observed acceleration relative to the predicted distribution for the cases both the acceleration phase ($a(t) \geq 1.0$ km/h/s) and the deceleration phase ($a(t) \leq -1.0$ km/h/s). By dividing the vehicle's percentile values into five bins, each separated by a 20 percentile for each trajectory, for both phases, a frequency distribution is created. Based on the pattern of the frequency distribution for both the acceleration and deceleration phases in each of the five bins, all trajectories are classified using the k-means method into various clusters.

Results of K-Means Clustering

The acceleration and deceleration phases of the trajectories are divided into two clusters, denoted as Cluster 0 and Cluster 1, respectively, as a result of the k-means clustering. The relative frequency of each bin for each cluster is depicted in a box plot in Figure 11. The box plot displays the outliers by dots, 0th percentile except for the outliers, 25th percentile, 50th percentile, 75th percentile, and 100th percentile except for the outliers by horizontal lines. In the acceleration phase, the "40% to 60%" bin corresponds to almost the median of the

acceleration distribution, the “0% to 20%” and “20% to 40%” bins correspond to weak acceleration, and the “60% to 80%” and “80% to 100%” bins correspond to strong acceleration. Similarly, in the deceleration phase, the “40% to 60%” bin is about the median of the acceleration distribution, the “0% to 20%” and “20% to 40%” bins correspond to strong deceleration, and the “60% to 80%” and “80% to 100%” bins correspond to weak deceleration. The percent of the observed percentile of the acceleration that falls in each bin is shown on the vertical axis.

Focusing on the differences in the box plots between clusters in each bin, we can find in the acceleration phase (Figure 11a) that in the “40% to 60%” bin the proportion of Cluster 1 is significantly higher than Cluster 0, while in the “80% to 100%” bin Cluster 0 has the much higher proportion. Cluster 1 drivers are more likely to take an acceleration value near the median of the distribution, suggesting that they are rather more timid than the drivers in Cluster 0. The significantly higher percentage of Cluster 0 drivers in the “80% to 100%” bin demonstrates that these drivers have a propensity to accept relatively strong acceleration. As a result, Cluster 1 can be interpreted as timid drivers, and Cluster 0 as aggressive drivers.

In the same manner, focusing on the deceleration phase shown in Figure 11b, it can be seen that Cluster 1 is remarkably higher in “0% to 20%” bin than Cluster 0, while Cluster 0 is higher than cluster 1 in the “20% to 40%” and “40% to 60%” bins. Since “0% to 20%” denotes a sharp deceleration, Cluster 1 is regarded as the over-reacting drivers, whereas Cluster 0 is regarded as the under-reacting drivers.

Categorization of Vehicles

From the above analysis, it is revealed that the time-series variation of percentile values can represent the characteristics of driving behavior. Then, to categorize the driving characteristics into timid and aggressive in the acceleration phase and under-reacting and over-reacting in the deceleration phase, we perform the cross-tabulation. The results are shown in Table 2. In the acceleration phase, the numbers of timid drivers and aggressive drivers are 723 and 465, respectively. In the deceleration phase, the numbers of under-reacting and over-reacting drivers are 575 and 513, respectively. Drivers who are under-reacting when decelerating and timid when accelerating may keep a long distance from the car ahead, while drivers who are over-reacting when decelerating and aggressive when accelerating may keep a shorter distance. According to Table 2, the timid and overreacting drivers are the second most prevalent among the four categories, while the aggressive

Table 2. Categorizing Each Trajectory

		Deceleration phase	
		Under-reacting	Over-reacting
Acceleration phase	Timid	362	261
	Aggressive	213	252

and under-reacting drivers, who may help stabilize traffic flow, are the least prevalent. The proportion of drivers in each of the four categories may influence traffic dynamics, such as capacity drop and oscillation, which should be investigated in a future work (34).

Time-Series Variations of Percentile Values

The analysis above suggests that the heterogeneity of driving behavior can be characterized by the percentile values within the predicted acceleration distribution, but to compute a vehicle acceleration behavior by using the proposed model, the sequential patterns of the percentile values need to be understood. Figure 12 demonstrates an example of an autocorrelogram of the percentile values of every 0.1 s of a vehicle entering the target section on the time 7.79 (see Figure 4) every 0.1 s during acceleration ($a(t) \leq -1.0$ km/h/s), deceleration ($a(t) \geq 1.0$ km/h/s), and constant speed (-1.0 km/h/s $< a(t) < 1.0$ km/h/s). In the figure, the shaded area represents the 95% confidence interval. It can be seen that the autocorrelations are not significant with the 95% confidence level regardless of driving state, except for the case where a time lag is 0.1 s. This trend can also be observed for most other vehicles. Therefore, correlations at every 0.1 s time step should be primarily considered in the simulation of driving behavior, but further analysis is needed because the characteristics of autocorrelations may also affect the traffic dynamics, such as the occurrence of stop-and-go wave.

Discussions and Conclusions

In recent years, it has been pointed out that stochastic fluctuations in car-following behavior caused by driver cognitive and operation errors in driving behavior have an essential effect on the traffic dynamics such as capacity drop and oscillation. For the convenience of mathematical processing, this stochasticity is typically represented by adding a random term that follows a normal distribution to the deterministic car-following model. However, the validity of the assumption that the stochastic term follows the normal distribution has not been investigated. In this study, the stochastic car-

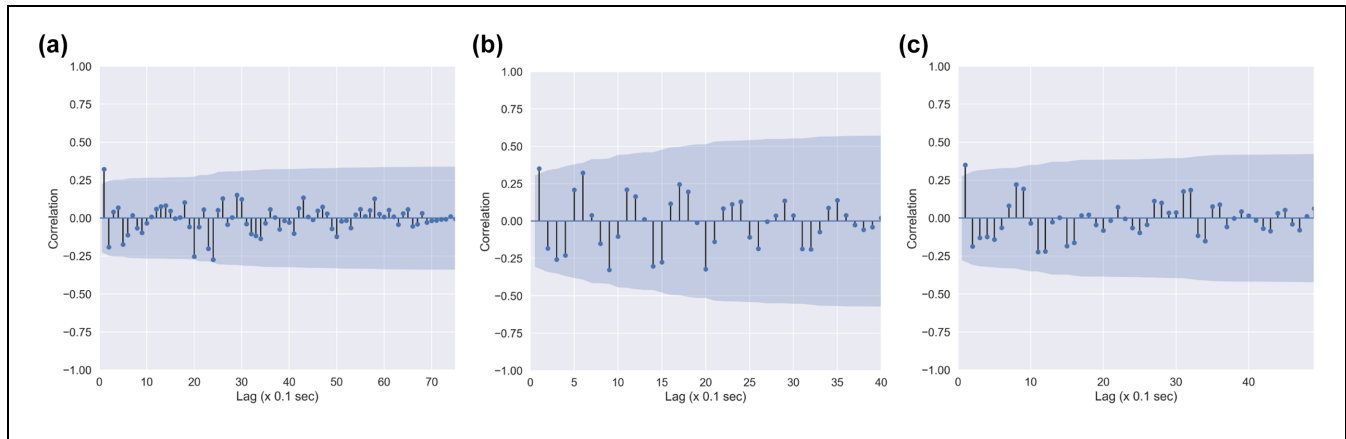


Figure 12. Autocorrelogram of time-series variations of percentile values: (a) acceleration, (b) deceleration, and (c) constant speed. Note: Shaded area = the 95% confidence interval.

following behavior was modeled using a data-driven approach without these presumptions. The proposed model predicts the probability distribution of acceleration by discretizing the observed acceleration. By using data on vehicle trajectories that were gathered on a freeway to train the model, we were able to accurately match the observed acceleration with the mean of the predicted probability distribution. Additionally, by the rolling horizon method using the developed model, we simulated the time-series variation of the acceleration for particular vehicles in free-flow state and congestion state. The results suggested that the model was able to reproduce the observed accelerations in both free and congested flows, and the observed values fell within the 95% confidence interval of the predicted distribution.

The relationship between the model's predicted probability distribution of acceleration and traffic conditions was then examined. The results demonstrated that the SD of the probability distribution tends to be large and multimodal at the generation of the stop-and-go wave as well as at the moments where vehicles go into and get out from stop-and-go waves. Additionally, it was established that, when moving at low speeds and needing significant acceleration and deceleration, the SD of the acceleration distribution is higher.

These findings imply that, in the aforementioned scenarios, driver perception and decision-making are subject to uncertainty. Such uncertainty may affect the macroscopic traffic properties such as oscillation and capacity drops, as previous research has shown. It implies that improving the stability of traffic flow can be achieved by controlling driving behavior to reduce these uncertainties. It can be achieved, for example, by providing some warnings and information calling drivers' attention. It has been noted that installing light emission devices on the hard shoulder at regular intervals and controlling

them to move slightly faster than the traffic flow has been successful in reducing traffic breakdowns and preventing capacity drops (36). It is believed to have the impact of lessening driver uncertainty and helping stabilize traffic flow.

Finally, the heterogeneity of driving behavior was analyzed based on the trend of variation in the percentile values of acceleration actually performed relative to the predicted probability distribution. As a result, the vehicles were found to fall into four categories: timid acceleration and under-reacting deceleration, timid acceleration and over-reacting deceleration, aggressive acceleration and under-reacting deceleration, and aggressive acceleration and over-reacting deceleration. In addition, we revealed that the autocorrelation with one-time step lag of percentile values within the predicted distribution is significant, implying that its correlation between a time step needs to be considered in calculating the acceleration behaviors in a simulation model.

In this paper, we focused on the analysis of the stochasticity and heterogeneity in the traffic dynamics based on the proposed model. As a future work, the computational method considering the autocorrelation should be developed for the microscopic traffic simulation by using this proposed car-following model, and the logical check whether it can work without any fatal error. Then, it should be verified that the proposed model can appropriately reproduce capacity drop and oscillation by conducting simulation experiments. It is also necessary to test the sensitivity of the vehicle category composition ratio to traffic dynamics to take measures to reduce traffic congestion and improve traffic safety on freeways. The proposed modeling approach discretizing vehicle behavior can be naturally extended to other driving behaviors such as merging and lane changing behaviors. This extension is one of the future directions.

This model is based on the data collected in a specific section, and it is not assured that the model is applicable to locations with different lane compositions and geometric features. Thus, the validation of the transferability of the model is required. In addition, the application of fine-tuning and transfer learning should be considered for extending the model to data from other locations.

Acknowledgments

The trajectory dataset is provided by Hanshin Expressway Co. Ltd. The authors would like to thank Enago (www.enago.jp) for the English language review.

Author Contributions

The authors confirm contribution to the paper as follows: study conception and design: Y. Shiomi, G. Li, V. Knoop; data collection: Y. Shiomi; analysis and interpretation of results: Y. Shiomi, G. Li, V. Knoop; draft manuscript preparation: Y. Shiomi. All authors reviewed the results and approved the final version of the manuscript.




Declaration of Conflicting Interests

The author(s) declared no potential conflicts of interest with respect to the research, authorship, and/or publication of this article.

Funding

The author(s) disclosed receipt of the following financial support for the research, authorship, and/or publication of this article: This work was supported by JSPS KAKENHI, grant numbers 19H02268 and 20KK0334.

ORCID iDs

Yasuhiro Shiomi  <https://orcid.org/0000-0002-7810-0971>
Guopeng Li  <https://orcid.org/0000-0003-4405-6332>
Victor L. Knoop  <https://orcid.org/0000-0001-7423-3841>

Data Accessibility Statement

The data used to support the findings of this study are available from the corresponding author on request.

References

- Haight, F. A. *Mathematical Theories of Traffic Flow*. Elsevier Science, 1963. <https://books.google.nl/books?id=U-AjInvo3sgC>.
- Wardrop, J. G. Some Theoretical Aspects of Road Traffic Research. *Proceedings of the Institution of Civil Engineers*, Vol. 1, No. 5, 1952, pp. 767–768. <https://doi.org/10.1680/ipeds.1952.11362>; <https://www.icevirtuallibrary.com/doi/10.1680/ipeds.1952.11362>.
- Branston, D. A Method of Estimating the Free Speed Distribution for a Road. *Transportation Science*, Vol. 13, No. 2, 1979, pp. 130–145. <http://www.jstor.org/stable/25767943>.
- Laval, J. A., C. S. Toth, and Y. Zhou. A Parsimonious Model for the Formation of Oscillations in Car-Following Models. *Transportation Research Part B: Methodological*, Vol. 70, 2014, pp. 228–238. <https://doi.org/10.1016/j.trb.2014.09.004>.
- Treiber, M., and A. Kesting. The Intelligent Driver Model with stochasticity – New insights into Traffic Flow Oscillations. *Transportation Research Part B: Methodological*, Vol. 117, 2018, pp. 613–623. <https://doi.org/10.1016/j.trb.2017.08.012>.
- Chen, D., J. Laval, Z. Zheng, and S. Ahn. A Behavioral Car-Following Model That Captures Traffic Oscillations. *Transportation Research Part B: Methodological*, Vol. 46, No. 6, 2012, pp. 744–761. <http://doi.org/10.1016/j.trb.2012.01.009>.
- Tian, J., H. M. Zhang, M. Treiber, R. Jiang, Z. Y. Gao, and B. Jia. On the Role of Speed Adaptation and Spacing Indifference in Traffic Instability: Evidence from Car-Following Experiments and its Stochastic Model. *Transportation Research Part B: Methodological*, Vol. 129, 2019, pp. 334–350. <https://doi.org/10.1016/j.trb.2019.09.014>.
- Xu, T., and J. Laval. Statistical Inference for Two-Regime Stochastic Car-Following Models. *Transportation Research Part B: Methodological*, Vol. 134, 2020, pp. 210–228. <https://doi.org/10.1016/j.trb.2020.02.003>.
- Yuan, K., J. Laval, V. L. Knoop, R. Jiang, and S. P. Hoogendoorn. A Geometric Brownian Motion Car-Following Model: Towards a Better Understanding of Capacity Drop. *Transportmetrica B*, Vol. 7, No. 1, 2019, pp. 915–927. <https://doi.org/10.1080/21680566.2018.1518169>.
- Ngoduy, D., S. Lee, M. Treiber, M. Keyvan-Ekbatani, and H. Vu. Langevin Method for a Continuous Stochastic Car-Following Model and its Stability Conditions. *Transportation Research Part C: Emerging Technologies*, Vol. 105, 2019, pp. 599–610. <https://doi.org/10.1016/j.trc.2019.06.005>; <https://www.sciencedirect.com/science/article/pii/S0968090X1831773X>.
- Ngoduy, D. Noise-Induced Instability of a Class of Stochastic Higher Order Continuum Traffic Models. *Transportation Research Part B: Methodological*, Vol. 150, 2021, pp. 260–278. <https://doi.org/10.1016/j.trb.2021.06.013>.
- Ossen, S., S. P. Hoogendoorn, and B. G. Gorte. Interdriver Differences in Car-Following a Vehicle Trajectory-Based Study. *Transportation Research Record: Journal of the Transportation Research Board*, 2006. 1965: 121–129.
- Hong, D., N. Uno, and F. Kurauchi. Heterogeneity in Multi-Anticipative Car-Following Behavior by Video Image Data. *International Journal of ITS Research*, Vol. 7, No.1, 2009, pp. 39–48.
- Berthoume, A. L., R. M. James, B. E. Hammit, C. Foreman, and C. L. Melson. Variations in Driver Behavior: An Analysis of Car-Following Behavior Heterogeneity as a Function of Road Type and Traffic Condition. *Transportation Research Record: Journal of the Transportation Research Board*, 2018. 2672: 31–44.
- Fadhoun, K., H. Rakha, A. Loulizi, and A. Abdelkefi. Vehicle Dynamics Model for Estimating Typical Vehicle Accelerations. *Transportation Research Record: Journal of the Transportation Research Board*, 2015. 2491: 61–71.

16. Makridis, M., G. Fontaras, B. Ciuffo, and K. Mattas. MFC Free-Flow Model: Introducing Vehicle Dynamics in Microsimulation. *Transportation Research Record: Journal of the Transportation Research Board*, 2019. 2673: 762–777.
17. Krajewski, R., J. Bock, L. Kloeker, and L. Eckstein. The highD Dataset: A Drone Dataset of Naturalistic Vehicle Trajectories on German Highways for Validation of Highly Automated Driving Systems. *Proc., 21st International Conference on Intelligent Transportation Systems (ITSC)*, Maui, HI, IEEE, New York, 2018, pp. 2118–2125. <https://doi.org/10.1109/ITSC.2018.8569552>.
18. Seo, T., Y. Tago, N. Shinkai, M. Nakanishi, J. Tanabe, D. Ushiroguchi, S. Kanamori, A. Abe, T. Kodama, S. Yoshimura, M. Ishihara, and W. Nakanishi. Evaluation of Large-Scale Complete Vehicle Trajectories Dataset on Two Kilometers Highway Segment for One Hour Duration: Zen Traffic Data. *Proc., International Symposium on Transportation Data and Modelling (ISTDM2021)*, Ann Arbor, MI, 2021.
19. Gilles, T., S. Sabatini, D. Tsishkou, B. Stanculescu, and F. Moutarde. HOME: Heatmap Output for Future Motion Estimation. *Proc., IEEE Conference on Intelligent Transportation Systems, Proceedings, ITSC*, Indianapolis, IN, September 19–22, 2021, IEEE, New York, pp. 500–507. <https://doi.org/10.1109/ITSC48978.2021.9564944>.
20. Zhou, M., X. Qu, and X. Li. A Recurrent Neural Network Based Microscopic Car Following Model to Predict Traffic Oscillation. *Transportation Research Part C: Emerging Technologies*, Vol. 84, 2017, pp. 245–264. <http://doi.org/10.1016/j.trc.2017.08.027>.
21. Fan, P., J. Guo, H. Zhao, J. S. Wijnands, and Y. Wang. Car-Following Modeling Incorporating Driving Memory Based on Autoencoder and Long Short-Term Memory Neural Networks. *Sustainability (Switzerland)*, Vol. 11, No. 23, p. 6755. <https://doi.org/10.3390/su11236755>.
22. Wang, X., R. Jiang, L. Li, Y. L. Lin, and F. Y. Wang. Long Memory is Important: A Test Study on Deep-Learning Based Car-Following Model. *Physica A: Statistical Mechanics and its Applications*, Vol. 514, 2019, pp. 786–795. <https://doi.org/10.1016/j.physa.2018.09.136>.
23. Lee, S., D. Ngoduy, and M. Keyvan-Ekbatani. Integrated Deep Learning and Stochastic Car-Following Model for Traffic Dynamics on Multi-Lane Freeways. *Transportation Research Part C: Emerging Technologies*, Vol. 106, 2019, pp. 360–377. <https://doi.org/10.1016/j.trc.2019.07.023>.
24. Zhang, X., J. Sun, X. Qi, and J. Sun. Simultaneous Modeling of Car-Following and Lane-Changing Behaviors Using Deep Learning. *Transportation Research Part C: Emerging Technologies*, Vol. 104, 2019, pp. 287–304. <https://doi.org/10.1016/j.trc.2019.05.021>.
25. Hochreiter, S., and J. Schmidhuber. Long Short-Term Memory. *Neural Computation*, Vol. 9, No. 8, 1997, pp. 1735–1780. <https://doi.org/10.1162/neco.1997.9.8.1735>.
26. Lin, T. Y., P. Goyal, R. Girshick, K. He, and P. Dollar. Focal Loss for Dense Object Detection. *IEEE Transactions on Pattern Analysis and Machine Intelligence*, Vol. 42, No. 2, 2020, pp. 318–327. <https://doi.org/10.1109/TPAMI.2018.2858826>.
27. Hoogendoorn, S. P., S. Ossen, and M. Schreuder. Empirics of Multianticipative Car-Following Behavior. *Transportation Research Record: Journal of the Transportation Research Board*, Vol. 1, No. 1965, 2006, pp. 112–120. <https://doi.org/10.3141/1965-12>.
28. Xu, Y., S. Bao, and A. K. Pradhan. Modeling Drivers' Reaction When Being Tailgated: A Random Forests Method. *Journal of Safety Research*, Vol. 78, 2021, pp. 28–35. <https://doi.org/10.1016/j.jsr.2021.05.004>.
29. Lenné, M. G., T. J. Triggs, and J. R. Redman. Time of Day Variations in Driving Performance. *Accident Analysis and Prevention*, Vol. 29, No. 4, 1997, pp. 431–437. [https://doi.org/10.1016/s0001-4575\(97\)00022-5](https://doi.org/10.1016/s0001-4575(97)00022-5).
30. Yeon, J., S. Hernandez, and L. Eleftheriadou. Differences in Freeway Capacity by Day of the Week, Time of Day, and Segment Type. *Journal of Transportation Engineering*, Vol. 135, No. 7, 2009, pp. 416–426. [https://doi.org/10.1061/\(ASCE\)0733-947X\(2009\)135:7\(416\)](https://doi.org/10.1061/(ASCE)0733-947X(2009)135:7(416)).
31. Ponnu, B., and B. Coifman. Speed-Spacing Dependency on Relative Speed from the Adjacent Lane: New Insights for Car Following Models. *Transportation Research Part B: Methodological*, Vol. 82, 2015, pp. 74–90. <http://doi.org/10.1016/j.trb.2015.09.012>.
32. Hartigan, J. A., and P. M. Hartigan. The Dip Test of Unimodality. *The Annals of Statistics*, Vol. 13, No. 1, 1985, pp. 70–84. <https://doi.org/10.1214/aos/1176346577>.
33. Hartigan, P. M. Computation of the Dip Statistic to Test for Unimodality. *Journal of the Royal Statistical Society. Series C (Applied Statistics)*, Vol. 34, No. 3, 1985, pp. 320–325. <https://doi.org/10.1214/aos/1176346577>.
34. Laval, J. A., and L. Leclercq. A Mechanism to Describe the Formation and Propagation of Stop-and-Go Waves in Congested Freeway Traffic. *Philosophical Transactions of the Royal Society A: Mathematical, Physical and Engineering Sciences*, Vol. 368, No. 1928, 2010, pp. 4519–4541. <https://doi.org/10.1098/rsta.2010.0138>.
35. Yeo, H., and A. Skabardonis. Understanding Stop-and-Go Traffic in View of Asymmetric Traffic Theory. In *Proc., Transportation and Traffic Theory 2009: Golden Jubilee: Papers Selected for Presentation at ISTTT18* (W. Lam, S. Wong, and H. Lo, eds.), 2009, Springer, Boston, MA, pp. 99–115. https://doi.org/10.1007/978-1-4419-0820-9_6.
36. Kameoka, H., H. Oneyama, M. Sakurai, and M. Tsuji. Effect of Dynamic Blink Control of Light-Emitting Devices Installed Along a Road Shoulder on Congestion Relief. *Journal of the Eastern Asia Society for Transportation Studies*, Vol. 11, No. 2011, 2015, pp. 1919–1930.